Journal of Power Sources 196 (2011) 8610–8617

Contents lists available at ScienceDirect

Journal of Power Sources

journal homepage: www.elsevier.com/locate/jpowsour

Nanosized $Li_4Ti_5O_{12}$/graphene hybrid materials with low polarization for high rate lithium ion batteries

Ying Shi, Lei Wen, Feng Li*, Hui-Ming Cheng

Shenyang National Laboratory for Materials Science, Institute of Metal Research, Chinese Academy of Sciences, 72 Wenhua Road, Shenyang 110016, PR China

ARTICLE INFO

Article history:
Received 16 March 2011
Received in revised form 25 May 2011
Accepted 1 June 2011
Available online 12 June 2011

Keywords:
Lithium titanate
Graphene
High rate anode materials
Lithium-ion batteries

ABSTRACT

We report a simple strategy to prepare a hybrid of lithium titanate ($Li_4Ti_5O_{12}$, LTO) nanoparticles well-dispersed on electrical conductive graphene nanosheets as an anode material for high rate lithium ion batteries. Lithium ion transport is facilitated by making pure phase $Li_4Ti_5O_{12}$ particles in a nanosize to shorten the ion transport path. Electron transport is improved by forming a conductive graphene network throughout the insulating $Li_4Ti_5O_{12}$ nanoparticles. The charge transfer resistance at the particle/electrolyte interface is reduced from 53.9 Ω to 36.2 Ω and the peak currents measured by a cyclic voltammogram are increased at each scan rate. The difference between charge and discharge plateau potentials becomes much smaller at all discharge rates because of lowered polarization. With 5 wt.% graphene, the hybrid materials deliver a specific capacity of 122 mAh g^{-1} even at a very high charge/discharge rate of 30 C and exhibit an excellent cycling performance, with the first discharge capacity of 132.2 mAh g^{-1} and less than 6% discharge capacity loss over 300 cycles at 20 C. The outstanding electrochemical performance and acceptable initial columbic efficiency of the nano-$Li_4Ti_5O_{12}$/graphene hybrid with 5 wt.% graphene make it a promising anode material for high rate lithium ion batteries.

1. Introduction

As one of the most important devices for energy storage, lithium ion batteries (LIBs) have many outstanding properties, such as high energy density, long cycle life, fast charging and discharging ability and friendliness to the environment. Therefore they have been widely used as power sources for portable electric devices. Nowadays LIBs are also expected to be a promising power source for electric vehicles (EV), hybrid vehicles (HEV) and plug-in hybrid vehicles (PHEV) [1–4]. To meet the dramatically increased demand for the emerging large-scale application of these EV, HEV and PHEV, electrode materials for LIBs with high safety, high power density and long cycle life are urgently required.

Among various anode materials for LIBs, spinel lithium titanate ($Li_4Ti_5O_{12}$, LTO) is considered an appealing candidate with its fast Li^+ insertion and de-insertion ability, excellent cycle reversibility, high safety and zero-strain during charging and discharging [5]. Compared with carbon-based anode materials, such as graphite, LTO exhibits a flatter operation potential plateau and higher operating voltage of about 1.55 V versus Li/Li^+, which can make the issue of lithium dendrite deposition on the surface of anode materials entirely resolved [6]. In addition, as the high equilibrium potential of the Ti^{4+}/Ti^{3+} redox couple is above the reduction potential of common electrolyte solvents, a solid electrolyte interface (SEI) film caused by solvent reduction does not form during the charge and discharge process. All of these merits make LTO more competitive as a safe anode material for high power LIBs. However, as LTO is an insulator [7], the low electrical conductivity becomes a major drawback which is unfavorable to high rate capability [8], because the polarization of the electrode becomes serious when charged/discharged at a higher current density. In order to overcome the low electrical conductivity and further improve the power performance of LTO material, many approaches have been developed. As nanosized particles can reduce the lithium-ion diffusion path, particle size reduction or special nanostructural design is effective in improving its rate capability [9–12]. Until now, various wet-chemical methods have been developed and used for the production of pure-phase nanosized $Li_4Ti_5O_{12}$ (n-LTO) particles, but agglomeration is usually inevitable during drying. Substituting the Ti^{4+} or Li^+ sites by an aliovalent metal is another important strategy for conductivity improvement. This is expected to produce a high reversible capacity as well as maintain a high rate performance [6,13,14]. Preparing a hybrid of LTO with a conductive second phase, such as noble metal nanoparticles [15] or metal oxides [16] and conductive carbonaceous materials [8,17–21], is also an effective way which has displayed significantly improved results.

Graphene, with an extraordinary electronic transport property, a flexible structure, high mechanical strength and high surface area

* Corresponding author. Tel.: +86 24 23971472; fax: +86 24 23903126.
E-mail address: fli@imr.ac.cn (F. Li).

0378-7753/$ – see front matter © 2011 Elsevier B.V. All rights reserved.
doi:10.1016/j.jpowsour.2011.06.002

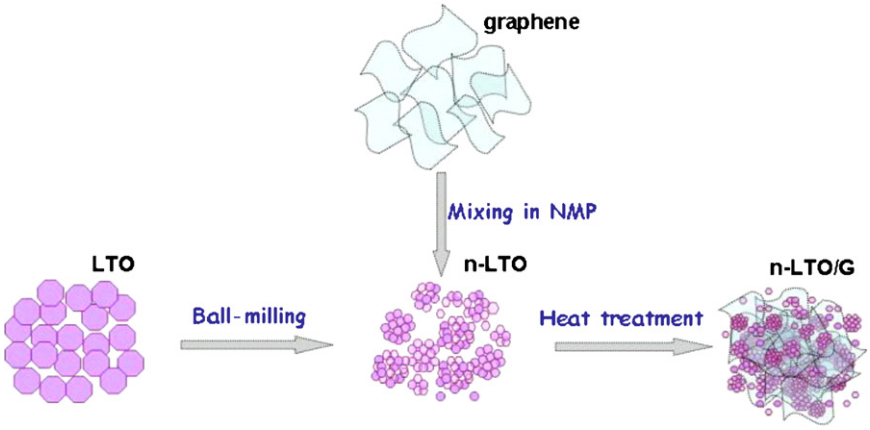

Fig. 1. Schematic of the preparation of the hybrid of n-LTO and graphene.

for improved interfacial contact [22–24], is regarded as an ideal conductive additive to nanostructured hybrids as electrodes of LIBs [25–30]. In addition, graphene produced by the chemical reduction of graphene oxide has abundant functional groups on the surface, such as –COOH and –OH, and thus may provide a better connection with other materials to form a homogenous composite or hybrid by interfacial interaction with some active particles during preparation [25,27]. In fact, the use of graphene to prepare hybrids cannot only increase electrical conductivity [23,29], but also improve the capacity and cyclic stability of anode materials [28]. Recently, Zhu et al. used graphene as a conductive additive to fabricate graphene-embedded LTO nanofibers [31], which showed great improved surface conductivity as well as rate capability. The graphene content was about 1 wt.% in the total carbon content of 7.2 wt.%, which suggests that the addition of only a small amount of graphene could play an important role in the hybrid. However, it is worth noting that the amount of graphene added in the hybrid is not a matter of the more the better, as it can affect the initial columbic efficiency of the electrode materials, a key factor in the practical application of LIBs. With the increase of graphene content, the irreversible capacity loss in the first cycle increases, which may be attributed to the formation of a SEI film and the reaction of oxygen-containing functional groups on graphene with lithium ions [32]. Therefore, how to balance the two effects of improving electrical conductivity and decreasing the initial efficiency that the graphene additive has on the LTO is another problem to be considered. In addition, in order to use the nanocomposite in large scale, a facile strategy for industrially effective production of the hybrid material with well improved properties also urgently need to be developed.

In this work, we prepared a hybrid of n-LTO that was well-dispersed on graphene nanosheets as an anode material for LIBs. Graphene is chosen as a conductive additive to form a well connected conductive network and reduce the difference between charge and discharge plateau potentials at all rates. It is found that the hybrid material exhibits significantly improved rate capability and cycling performance. The relationship between initial columbic efficiency and graphene content in the hybrid is also taken into consideration. With 5 wt.% graphene content, the hybrid material shows outstanding performance as an anode material in LIBs.

2. Experimental

2.1. Material synthesis

LTO with 99.5% purity and about 2 μm average particle diameter was used as the raw material. For the fabrication of n-LTO particles,

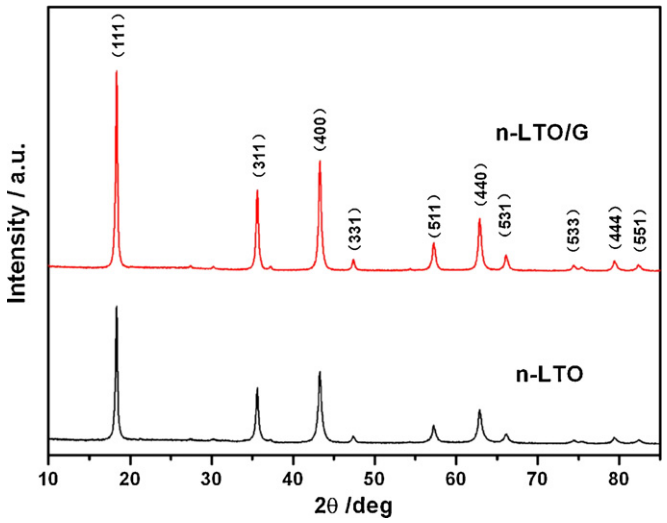

Fig. 2. XRD patterns of n-LTO and n-LTO/G hybrids.

ultrafine ball milling was carried out for 1.5 h with alcohol as dispersant. A uniformly dispersed graphene (reduced from graphene oxide) solution using *N*-methyl-2-pyrrolidine (NMP) as dispersant was mixed with the n-LTO material to give 5 wt. % graphene in

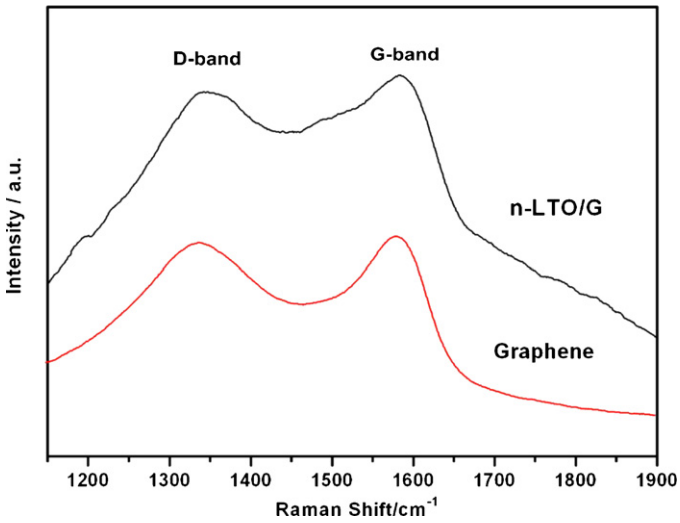

Fig. 3. Raman spectra of the n-LTO/G hybrid and graphene.

the hybrid, which was used for most of the study unless otherwise mentioned, and samples with other amounts of graphene were produced in the same way. After 1 h vigorous stirring, the mixture was heated at 200 °C to remove the solvent and ground in a mortar. The sample was then further heated to 500 °C and annealed for 4 h in an Ar atmosphere for healing the defects of LTO during ball milling and for reduction of reduced graphene oxide. Finally, a grey powder of n-LTO/G hybrid was obtained.

2.2. Materials characterization

The structures of the n-LTO and n-LTO/G hybrid were characterized by scanning electron microscopy (SEM, FEI Nova Nano 430) and transmission electron microscopy (Tecnai F20, 200 kV). Phase identification was characterized by X-ray powder diffraction measurements using a D/max 2400 with Cu Kα (1.54 Å) radiation, X-ray photoelectron spectroscopy measurements (Escalab 250, Al Kα) and Raman spectroscopy (JY Labram HR 800) using 632.8 nm excited laser. The amount of graphene in the n-LTO/G hybrid was measured by thermogravimetry at a heating rate of 10 °C min^{-1} in air from 40 °C to 1000 °C by Netzsch-STA 449 C.

2.3. Electrochemical measurements

The charge–discharge properties of the samples were measured by assembling half cells in a glove box filled with Ar gas. The working electrode was prepared as follows: first, active material (80 wt.%), acetylene black (10 wt.%) and polyvinylidene fluoride binder (10 wt.%) were mixed and ground with NMP as solvent to form a uniform slurry, then coated onto an aluminum foil and dried under vacuum at 120 °C for 12 h After the foil was cut into disks (13 mm in diameter) and pressed, coin cells were assembled with lithium metal as the counter electrode and a Celgard 2400 membrane as separator. The electrolyte was 1 M $LiPF_6$, ethylene carbonate:dimethyl carbonate = 1:1 in volume ratio. Galvanostatic discharge–charge measurements were carried out under different current densities between 0.8 and 2.5 V (vs. Li/Li^+) with a cell test instrument (LAND Electronic Co., China) at room temperature. Cyclic voltammograms were recorded from 0.8 to 2.5 V at different scanning rates using a Solartron 1287 electrochemical workstation, and the AC impedance spectrum was measured by a Solatron 1260 Impedance Analyzer in the frequency range from 10 mHz to 100 kHz with a potential perturbation at 10 mV. All the LIB measurements mentioned above are based on the total mass of the active material.

3. Results and discussion

3.1. Synthesis and characterization of the n-LTO and n-LTO/G hybrid

Fig. 1 illustrates the preparation of n-LTO and its graphene hybrid. n-LTO particles were obtained by ball milling micrometer-sized LTO, then mixed with graphene in a NMP solution. After drying and heating at 500 °C, a nano-$Li_4Ti_5O_{12}$/graphene (n-LTO/G) hybrid was obtained. Heat treatment used here is to repair the defects of LTO resulted from the ball-milling procedure, as well as further reducing the graphene to obtain higher conductivity. Fig. 2 shows the X-ray diffraction (XRD) spectra of the hybrid. All peaks can be indexed as spinel LTO according to JCPDS File No. 26-1198 and no impurity peaks can be found. These results indicate that the addition of graphene has no effect on the crystal structure of spinel LTO. The quantity of the added graphene measured by TG in air atmosphere is about 5 wt.%. However, the D and G peaks are clearly observed in the Raman spectra and are similar to those of pure graphene shown in Fig. 3, which indicates that the structure of graphene is maintained during the preparation procedure.

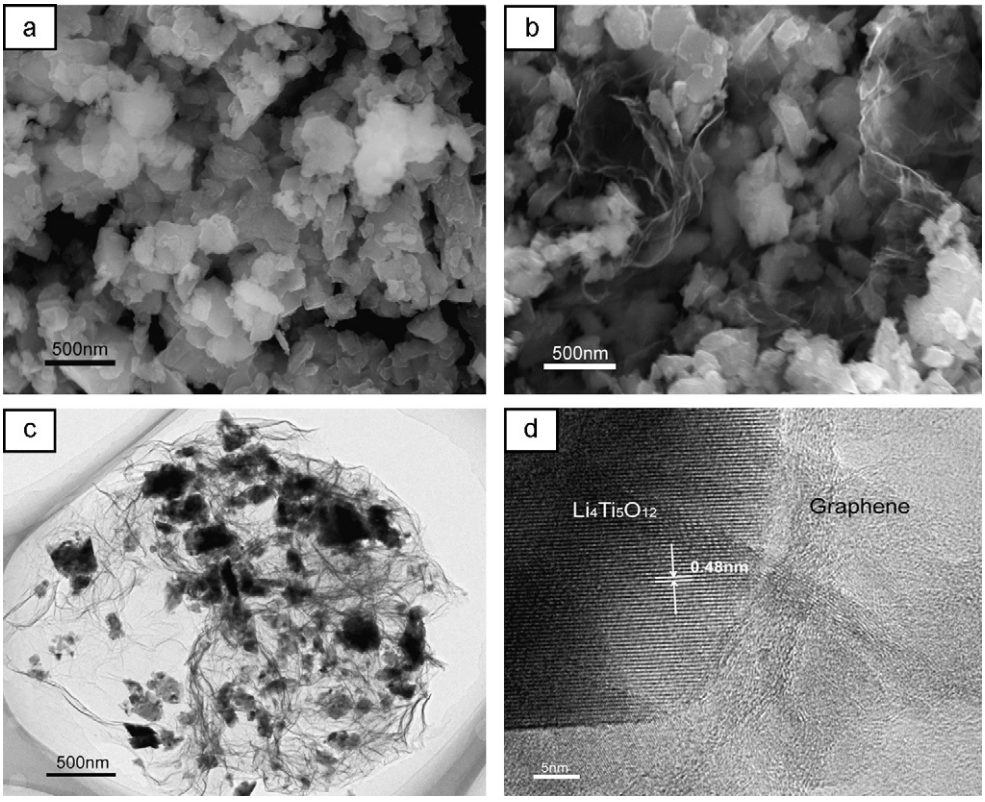

Fig. 4. SEM images of (a) n-LTO and (b) n-LTO/G hybrid, and (c and d) TEM images of the n-LTO/G hybrid at different magnifications.

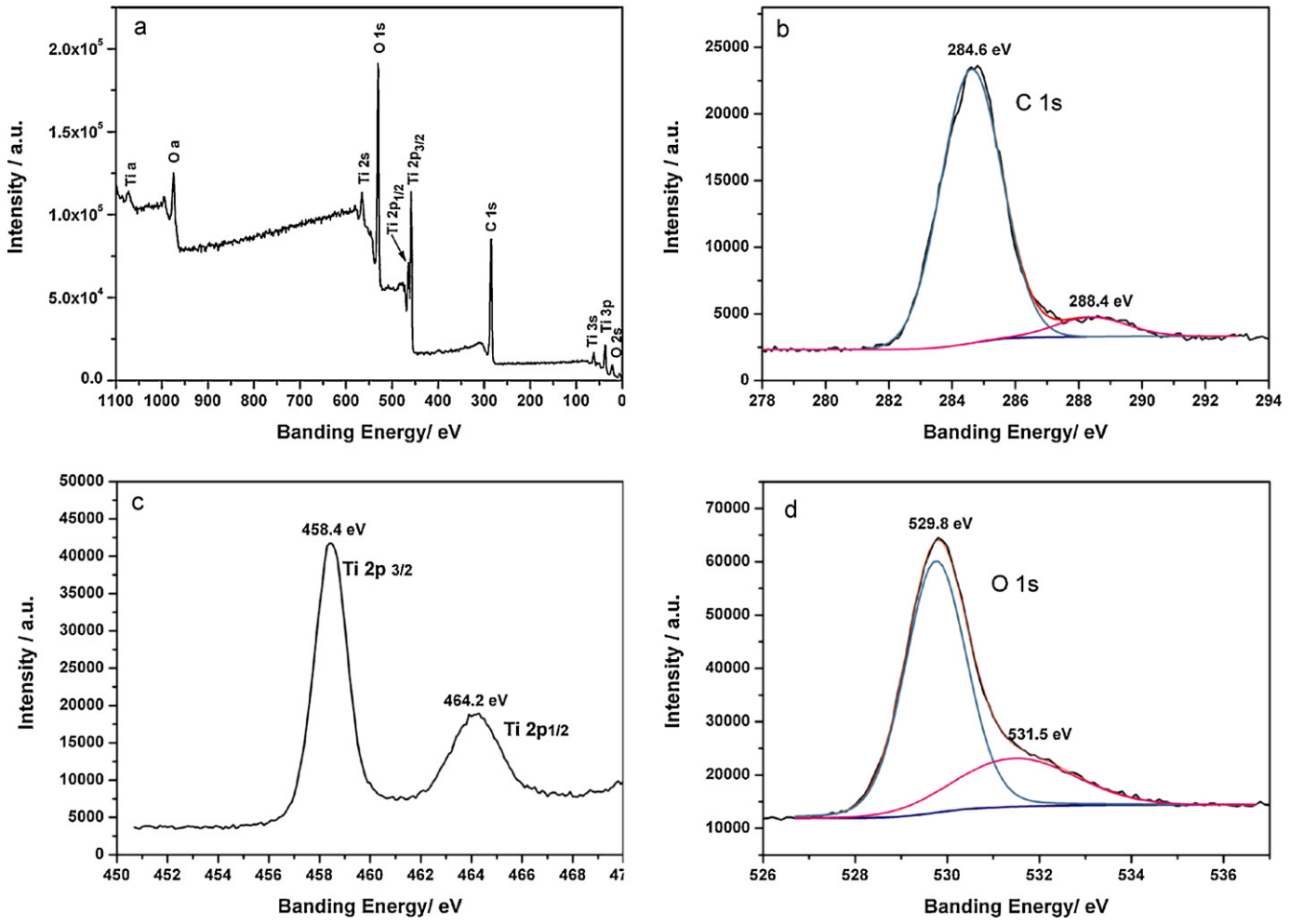

Fig. 5. (a) XPS spectrum of the n-LTO/G hybrid, and (b) C 1s, (c) Ti 2p and (d) O 1s spectra of the hybrid.

The n-LTO particles after ball-milling are about 100–400 nm in size, as shown in Fig. 4a, and some of them are aggregated. From the images of the n-LTO/G hybrid (Fig. 4b and c), it can be seen that the n-LTO particles are well dispersed among the graphene nanosheets, and the graphene extends in all directions like a stretched network, giving a conductive connection between the insulating LTO particles. The contact between LTO and graphene nanosheets can be observed from the high resolution TEM image shown in Fig. 4d. The LTO particles have a well-crystallized structure with 0.48 nm lattice spacing, consistent with the lattice spacing of (1 1 1) plane. This provides further evidence for the phase purity, while the graphene nanosheets firmly contact with the LTO particles, giving a better connection between adjacent LTO particles, as well as preventing them from further aggregation.

Fig. 5 shows the XPS measurements of the n-LTO/G hybrid. The C 1s peak at 284.6 eV observed in Fig. 5b is related to graphitical carbon in graphene, while the O 1s peak at 529.8 eV shown in Fig. 5d is associated with Ti–O band in the LTO. The small C 1s (288.4 eV) peak as well as the small O 1s (531.5 eV) peak in the spectrum indicate the presence of residual oxygen containing groups bonded with C atoms (such as carbonyl group) in graphene. However, it is worth noting that neither 281.5 eV peak in the C 1s spectrum nor 454.9 eV peak in the Ti 2p spectrum, corresponding to the C 1s and Ti $2p_{3/2}$ spin orbital peaks of TiC, can be observed in the XPS results of the hybrid. This suggests no bond is formed between the n-LTO particles and the graphene sheets.

3.2. Electrochemical performance

The electrochemical performance of the n-LTO/G hybrid was characterized by cyclic voltammograms (CV) within a potential window of 0.8–2.5 V (vs. Li/Li^+). It is widely known that the shapes of redox peaks observed in a CV curve can reflect the electrochemical reaction kinetics of Li^+ insertion/deinsertion. A sharp and well-resolved peak generally signifies fast Li^+ insertion/deinsertion, whereas a broad peak suggests a sluggish process. From the CV comparison shown in Fig. 6a, it can be seen that the CV curves of n-LTO have broadened with the increase of scan rate, while those of the hybrid with graphene have retained a stable shape. In addition, all the peak currents of the n-LTO/G hybrid are higher than those of the n-LTO at each scan rate. The relation between peak currents and scan rates can indicate the electrochemical reaction characteristics [33–35]. For the diffusion-limited process, the peak current is proportional to the square roots of the scan rate ($\nu^{1/2}$) as the followed equation:

$$i_p = 2.69 \times 10^5 n^{3/2} D^{1/2} C \nu^{1/2}$$

Where D is the diffusion coefficient, C is concentration of the reactant and n represents the number of transfer electrons. In our experiment, linear correlation between peak currents and the square roots of the scan rate in the cathodic process can be observed from both n-LTO and n-LTO/G hybrid, as shown in Fig. 6b, which signifies obvious diffusion-controlled electrode process. Furthermore,

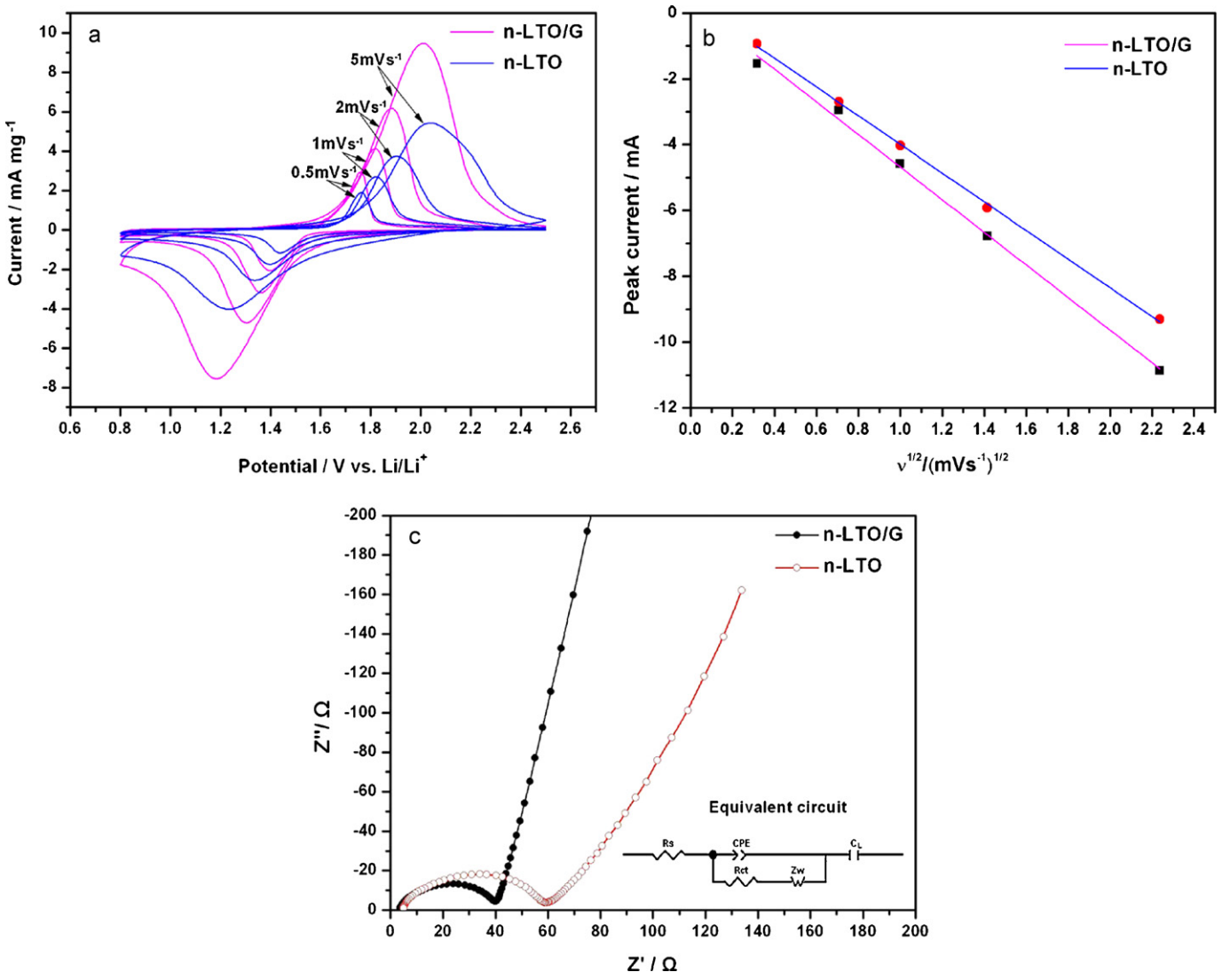

Fig. 6. (a) Cyclic voltammograms of the n-LTO and n-LTO/G electrodes, (b) cathodic peak currents against square roots of scan rate for the n-LTO and n-LTO/G electrodes and (c) AC impedance spectra with the equivalent circuit from the EIS measurements (inset).

the slope of the fitted line is dependent on the diffusion coefficient in the equation about the peak current and scan rate. Therefore it can be deduced that the n-LTO/G hybrid had higher diffusion coefficient by the comparison of the slopes of these two straight lines. These results demonstrate that the addition of graphene can effectively improve the electrochemical reaction kinetics of Li^+ insertion/deinsertion. The AC impedance spectra of the n-LTO and n-LTO/G electrodes shown in Fig. 6c were also measured to examine the kinetic processes. The intercept impedance on the *Z*-real axis reflects the electrolyte solution resistance, while the semicircle in the high–middle frequency range and the oblique line at low frequencies represents the charge-transfer process and the lithium ion diffusion process, respectively. These AC impedance spectra were fitted by a simple modified Randles–Ershler equivalent circuit [36], shown in the inset of the figure. Here R_s is the resistance of the electrolyte, R_{ct} the charge transfer resistance at the particle/electrolyte interface, and Z_W the Warburg impedance. A constant phase element, abbreviated to CPE, is placed to represent the double-layer capacitance. C_L is the insertion capacitance at the applied potential. Table 1 shows the parameters of the recorded equivalent circuit, from which we can see that both R_s and R_{ct} of the n-LTO/G hybrid are smaller than those of the n-LTO electrode, whereas the exchange current density ($i_0 = RT/nFR_{ct}$) of the n-LTO/G electrode is higher than that of the n-LTO electrode. This lowered electrical resistance for the n-LTO/G electrode further proves that the addition of graphene, even at a small amount (5 wt.%), can give a great improvement by increasing the electrical conductivity of the insulating LTO particles, which is consistent with the result of the comparison of CV curves.

Fig. 7 shows the charge and discharge curves of the n-LTO and n-LTO/G electrodes at different rates from 1 C to 30 C. For the n-LTO/G hybrid shown in Fig. 7b, the discharge capacity is 171.7 mAh g^{-1} at 1 C, very close to the theoretical value (175 mAh g^{-1}) [10], while it is only 159.7 mAh g^{-1} for the n-LTO shown in Fig. 7a. In addition, the n-LTO/G always shows a higher discharge capacity than the n-LTO regardless of the rate as shown in Fig. 7c. It should be specially noted that, although the reversible capacity of graphene is much higher than that of LTO, the contribution to the capacity of n-LTO/G hybrid from graphene is negligible due to the high dis-

Table 1
Impedance parameters calculated from equivalent circuits.

Materials	R_s (Ω)	R_{ct} (Ω)	i_0 (mA cm^{-2})
n-LTO	4.2	53.9	0.48
n-LTO/G	3.2	36.2	0.71

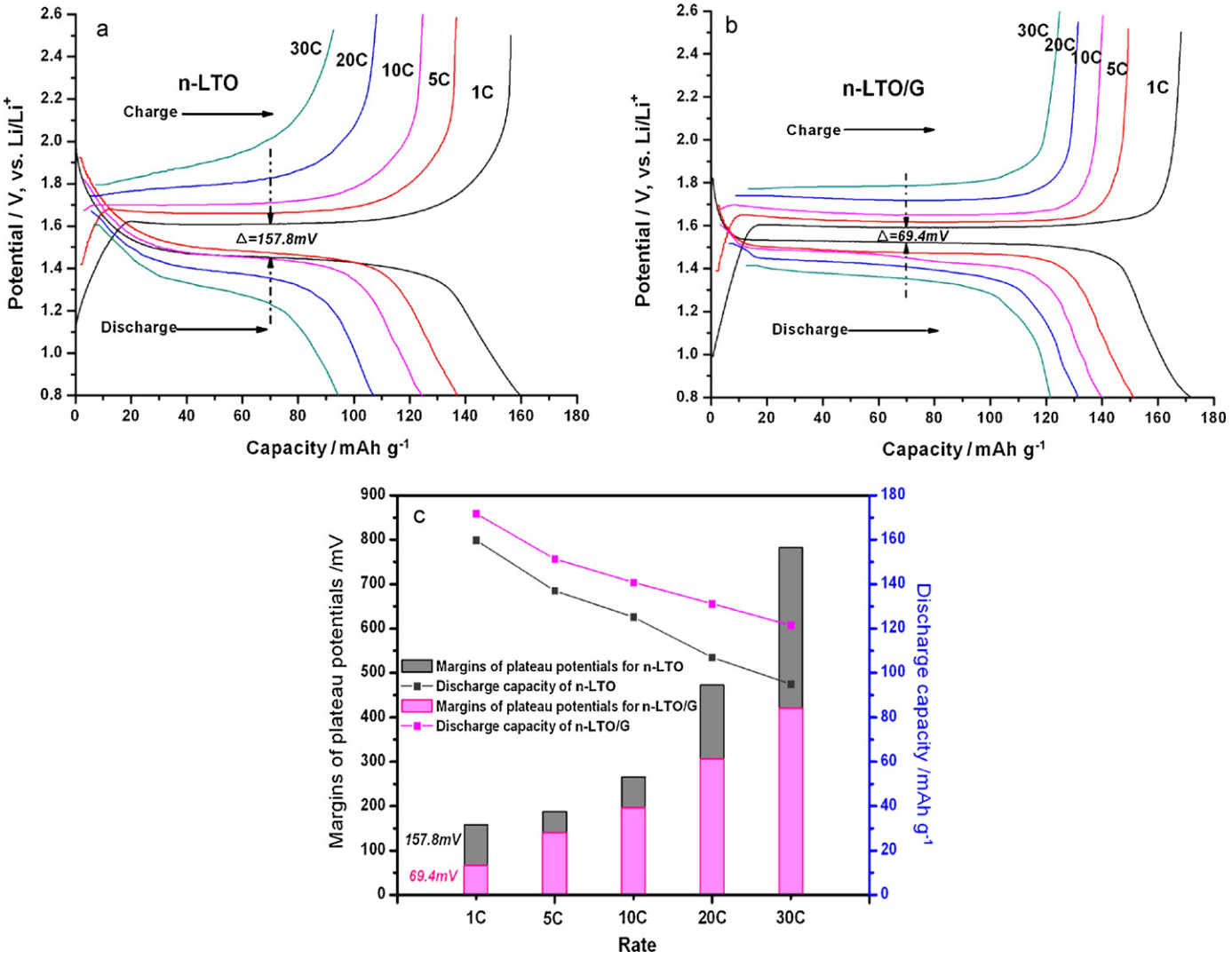

Fig. 7. Charge and discharge curves of (a) n-LTO and (b) n-LTO/G electrodes at 1 C, 5 C, 10 C, 20 C, and 30 C, and (c) comparison of the charge and discharge plateau potential difference.

charge cut-off potential (0.8 V) and the small amount of graphene added (5 wt.%). From these charge/discharge curves, we can also see that when charged/discharged at low rates, such as 1 C and 5 C, both electrodes exhibit a flat operation potential plateau. However, with the rate increased, the potential plateau of the n-LTO becomes shorter and gradually bends down while that of the n-LTO/G electrode still remains flat. This is because, at an increased rate, the polarization of the n-LTO without graphene would be increased. A comparison of the margins of the plateau potentials was taken for the two electrodes shown in Fig. 7c. Here the value of the margin is the potential difference between the charge and discharge plateau potentials, and this potential difference can represent the degree of polarization of the electrode. As shown in this figure, the values of the margin for the n-LTO/G electrode are much smaller than those of the n-LTO electrode at all discharge rates from 1 C to 30 C, which again indicates that the n-LTO/G electrode has lower polarization and better reaction kinetics, because of the improved electrical conductivity produced by the graphene in the hybrid.

The charge and discharge specific capacity with number of cycles for the n-LTO/G hybrid and n-LTO particles at different rates from 1 C to 30 C are shown in Fig. 8a. Both electrodes display good cyclic performance at each rate, which may be attributed to the stable cycle life of pure LTO as reported earlier [11,37,38]. Compared with the n-LTO, the n-LTO/G electrode exhibits higher specific capacity and much better rate capability as shown in Fig. 8a. The capacity difference between the two samples can be clearly seen and becomes larger at larger rates. For instance, at a 1 C rate, the discharge specific capacity of the n-LTO/G is about 170 mAh g^{-1}, nearly 10 mAh g^{-1} higher than that of the n-LTO sample, while at 30 C the discharge specific capacity is about 122 mAh g^{-1} for n-LTO/G and 92 mAh g^{-1} for the n-LTO, with the capacity difference three times bigger. This improved high rate capability of the n-LTO/G electrode could be explained mainly by the reduced resistance and polarization of the electrode, as described above. With a graphene conductive network throughout the whole hybrid material, many more pathways for electron transport are produced, thus the electron transport is more effective and the electrical conductivity of the electrode is improved. Fig. 8b shows the cyclic performance of the n-LTO/G hybrid at 20 C. A stable cycle life can be observed from this curve. In the first cycle, the discharge capacity was 132.2 mAh g^{-1}, and after 300 charge/discharge cycles it still remains at 124.0 mAh g^{-1}, a 94.8% retention of the first discharge capacity.

Based on the aforesaid experimental results, it can be proved that the electrochemical performance of LTO is significantly improved by the addition of graphene. However, to improve the electrochemical performance simply by increasing the graphene content in the hybrid is not advisable, because the initial columbic

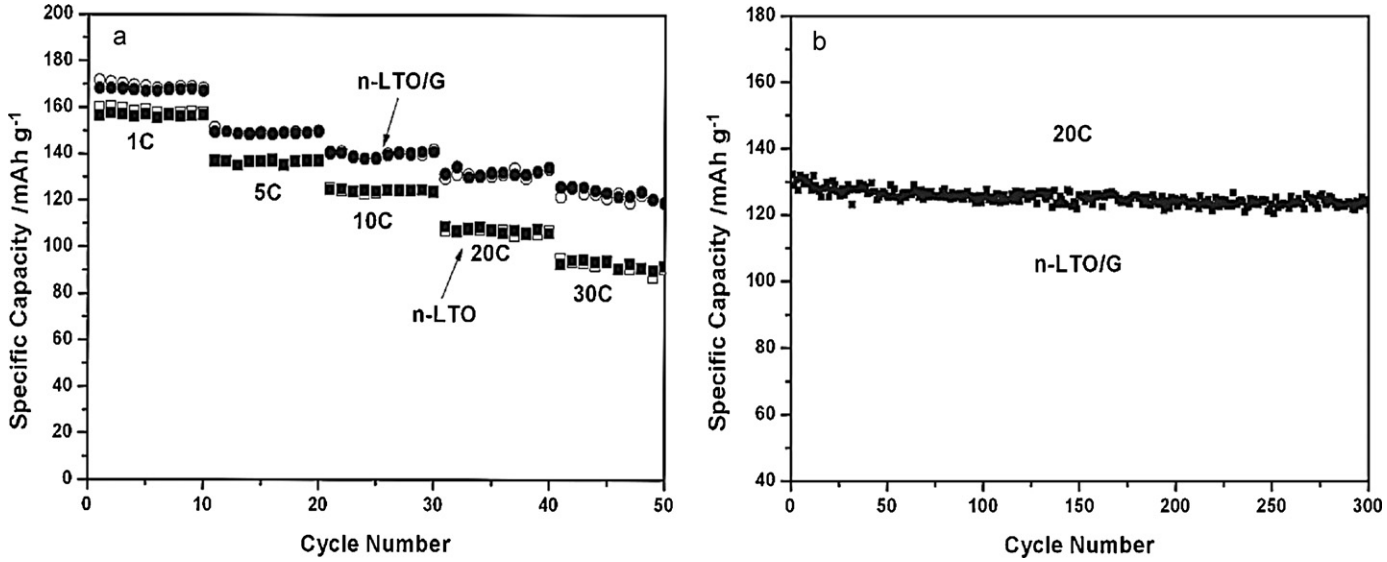

Fig. 8. (a) Specific capacity of the n-LTO and n-LTO/G at different charge/discharge rates and (b) cyclic performance of n-LTO/G at 20 C.

efficiency also plays a very important role in the practical application of LIBs. Thus there must be a trade-off between the electrical conductivity and the initial columbic efficiency. In the previous investigations on the preparation of improved electrode materials, graphene has been added with an amount from 0.5 wt.% to 40 wt.% [20,27–29]. Though the electrochemical properties were all reported to be greatly increased, their initial columbic efficiency varied greatly, and some showed a value no more than 70%. In order to find an approximate relationship between the content of graphene and the initial columbic efficiency, electrodes with four different additions of graphene were compared, and the results shown in Fig. 9 are in agreement with expectations. A high content of graphene led to a decreased initial columbic efficiency although it could increase the first discharge capacity due to the irreversible capacity of graphene and improve the conductivity of the hybrid. This demonstrates that, when graphene is used as a conductive additive, the amount added should be taken into consideration from both the electrical conductivity and initial columbic efficiency aspects described above. From our results, 5 wt.% of added graphene in n-LTO can provide an improved electrochemical performance with an acceptable initial columbic efficiency, which is appropriate for the practical application of LIBs.

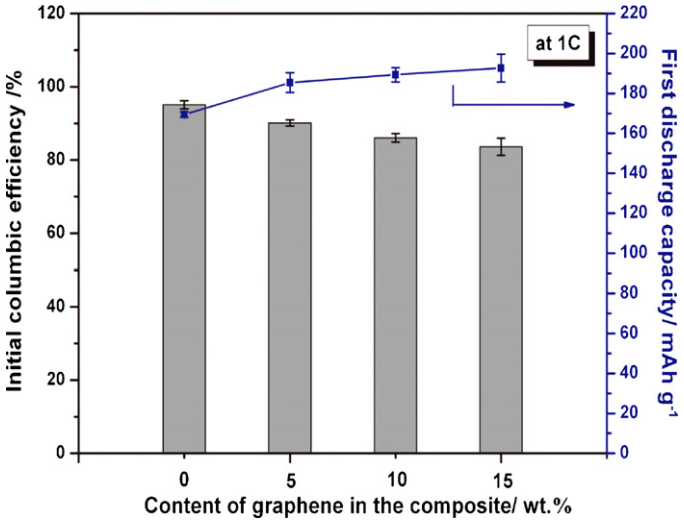

Fig. 9. Comparison of initial columbic efficiency with different contents of graphene in the hybrid.

4. Conclusions

We prepared a hybrid material of n-LTO/G by incorporating n-LTO particles on graphene sheets. The graphene sheets were used as a conductive additive and have formed a conducting network among the insulating n-LTO particles, which facilitates electron transport. The n-LTO/G hybrid exhibits obviously improved electrical conductivity, rate capability and cyclic stability compared with the pure n-LTO. 5 wt.% graphene in the n-LTO/G hybrid not only effectively reduces the resistance and polarization of the electrode, but also properly balances the two effects that graphene has on both electrical conductivity and initial columbic efficiency of the hybrid. This excellent electrochemical performance makes n-LTO/G hybrid a promising anode material for high-rate lithium ion batteries and this simple preparation method enables its production on a large scale.

Acknowledgements

This work was supported by Ministry of Science and Technology of China (No. 2009AA03Z337), National Science Foundation of China (Nos. 50921004 and 50632040), and Chinese Academy of Sciences (No. KJCX2-YW-231). The authors thank Dr. G. Liu and Mr. G.M. Zhou and Miss N. Li for helpful discussion and Dr. D.M. Tang for his help in TEM characterization.

References

[1] R.F. Nelson, J. Power Sources 91 (2000) 2–26.
[2] M. Armand, J.M. Tarascon, Nature 451 (2008) 652–657.
[3] B. Kang, G. Ceder, Nature 458 (2009) 190–193.
[4] J.M. Tarascon, M. Armand, Nature 414 (2001) 359–367.
[5] T. Ohzuku, A. Ueda, N. Yamamoto, J. Electrochem. Soc. 142 (1995) 1431–1435.
[6] T.F. Yi, L.J. Jiang, J. Shu, C.B. Yue, R.S. Zhu, H.B. Qiao, J. Phys. Chem. Solids 71 (2010) 1236–1242.
[7] M.R. Harrison, P.P. Edwards, J.B. Goodenough, Philos. Mag. B 52 (1985) 679–699.
[8] X. Li, M.Z. Qu, Y.J. Huai, Z.L. Yu, Electrochim. Acta 55 (2010) 2978–2982.
[9] E.M. Sorensen, S.J. Barry, H.K. Jung, J.R. Rondinelli, J.T. Vaughey, K.R. Poeppelmeier, Chem. Mater. 18 (2006) 482–489.
[10] L. Kavan, M. Gratzel, Electrochem. Solid State Lett. 5 (2002) A39–A42.
[11] C. Jiang, M. Ichihara, I. Honma, H.S. Zhou, Electrochim. Acta 52 (2007) 6470–6475.
[12] J.R. Li, Z.L. Tang, Z.T. Zhang, Electrochem. Commun. 7 (2005) 894–899.

[13] S.H. Huang, Z.Y. Wen, X.J. Zhu, Z.X. Lin, J. Power Sources 165 (2007) 408–412.
[14] J. Wolfenstine, J.L. Allen, J. Power Sources 180 (2008) 582–585.
[15] S.H. Huang, Z.Y. Wen, J.C. Zhang, X.L. Yang, Electrochim. Acta 52 (2007) 3704–3708.
[16] Y.Y. Wang, Y.J. Hao, Q.Y. Lai, J.Z. Lu, Y.D. Chen, X.Y. Ji, Ionics 14 (2008) 85–88.
[17] J. Gao, J.R. Ying, C.Y. Jiang, C.R. Wan, J. Power Sources 166 (2007) 255–259.
[18] G.J. Wang, J. Gao, L.J. Fu, N.H. Zhao, Y.P. Wu, T. Takamura, J. Power Sources 174 (2007) 1109–1112.
[19] J.J. Huang, Z.Y. Jiang, Electrochim. Acta 53 (2008) 7756–7759.
[20] L. Cheng, J. Yan, G.N. Zhu, J.Y. Luo, C.X. Wang, Y.Y. Xia, J. Mater. Chem. 20 (2010) 595–602.
[21] H.Y. Yu, X.F. Zhang, A.F. Jalbout, X.D. Yan, X.M. Pan, H.M. Xie, R.S. Wang, Electrochim. Acta 53 (2008) 4200–4204.
[22] A.K. Geim, K.S. Novoselov, Nat. Mater. 6 (2007) 183–191.
[23] S. Stankovich, D.A. Dikin, G.H.B. Dommett, K.M. Kohlhaas, E.J. Zimney, E.A. Stach, R.D. Piner, S.T. Nguyen, R.S. Ruoff, Nature 442 (2006) 282–286.
[24] A.K. Geim, Science 324 (2009) 1530–1534.
[25] G.M. Zhou, D.W. Wang, F. Li, L.L. Zhang, N. Li, Z.S. Wu, L. Wen, G.Q. Lu, H.M. Cheng, Chem. Mater. 22 (2010) 5306–5313.
[26] Y. Ding, Y. Jiang, F. Xu, J. Yin, H. Ren, Q. Zhuo, Z. Long, P. Zhang, Electrochem. Commun. 12 (2010) 10–13.
[27] Z.S. Wu, W.C. Ren, L. Wen, L.B. Gao, J.P. Zhao, Z.P. Chen, G.M. Zhou, F. Li, H.M. Cheng, ACS Nano 4 (2010) 3187–3194.
[28] S.M. Paek, E. Yoo, I. Honma, Nano Lett. 9 (2009) 72–75.
[29] D.H. Wang, D.W. Choi, J. Li, Z.G. Yang, Z.M. Nie, R. Kou, D.H. Hu, C.M. Wang, L.V. Saraf, J.G. Zhang, I.A. Aksay, J. Liu, ACS Nano 3 (2009) 907–914.
[30] M.H. Liang, L.J. Zhi, J. Mater. Chem. 19 (2009) 5871–5878.
[31] N. Zhu, W. Liu, M.Q. Xue, Z.A. Xie, D. Zhao, M.N. Zhang, J.T. Chen, T.B. Cao, Electrochim. Acta 55 (2010) 5813–5818.
[32] P. Guo, H.H. Song, X.H. Chen, Electrochem. Commun. 11 (2009) 1320–1324.
[33] X.J. Wang, L. Wang, J.J. Wang, T. Chen, J. Phys. Chem. B 108 (2004) 5627–5633.
[34] C. Lai, Y.Y. Dou, X. Li, X.P. Gao, J. Power Sources 195 (2010) 3676–3679.
[35] K.R. Prasad, N. Munichandraiah, Synth. Met. 130 (2002) 17–26.
[36] K. Dokko, M. Mohamedi, M. Umeda, I. Uchida, J. Electrochem. Soc. 150 (2003) A425–A429.
[37] C.H. Jiang, E. Hosono, M. Ichihara, I. Honma, H.S. Zhou, J. Electrochem. Soc. 155 (2008) A553–A556.
[38] J. Kim, J. Cho, Electrochem. Solid State Lett. 10 (2007) A81–A84.